A Helical Peptide Receptor for [60]Fullerene

Alberto Bianco,[a] Carlo Corvaja,[b] Marco Crisma,[a] Dirk M. Guldi,[c] Michele Maggini,[a] Elena Sartori,[b] and Claudio Toniolo*[a]

Abstract: Two terminally blocked nonapeptides, each made up of six Aib residues, a Gly spacer and two L-Tyr residues in positions 2 and 8 (these are substituted in the side chain with either ferrocenoyl or methyl moieties), have been synthesized by solution methods and fully characterized. FT-IR absorption and two-dimensional NMR analyses indicate that a 3_{10}-helical conformation is adopted by these rigid peptides in structure-supporting solvents. An X-ray diffraction investigation shows that the bis-L-Tyr(Me) nonapeptide in the crystal state is folded in a regular right-handed 3_{10}-helical structure. As five amino acid units separate the two substituted L-Tyr residues in the peptide sequence, the two side chain moieties will—in solution—face each other after two complete turns of the ternary helix. By carrying out a detailed photophysical analysis, we have demonstrated that the electron-rich, hydrophobic and wide cavity generated by the nonapeptide template with two ferrocenoyloxybenzyl walls is able to host [60]fullerene. Further evidence for this superstructure has been provided in the gas phase by a mass spectrometric investigation.

Keywords: conformation analysis · fullerenes · peptides · photoinduced processes · receptors

Introduction

Detailed understanding of the electronic interactions between noncovalently assembled donor–acceptor partners is heavily based on the design of molecular structures with well defined geometries. It has been demonstrated that peptides rich in Aib (α-aminoisobutyric acid) tend to adopt ordered secondary structures (β-turns[1] and 3_{10}-/α-helices[2]) of remarkable stability.[3] As guest (even side chain-functionalized) amino acids can be easily accommodated within a sequence of host Aib residues, it is possible to predict the reciprocal spatial relationship of the guests to good approximations on the basis of their relative sequence positions.[4] In this context, Aib-rich peptides have been exploited to study intramolecular radical–radical interactions and fluorescence quenching and redox processes originated by probes located in close proximity within rigid turns or helical structures.[5, 6]

Rational design of Aib-based peptide templates has also been used to catalyse organic reactions[7] and in molecular recognition studies. In the latter type of application, a series of Aib-rich nonapeptides containing two side chain-modified L-Tyr residues, separated by five intervening amino acids, have been preliminarily investigated as [60]fullerene receptors through the use of HPLC and a silica-bound fullerene derivative.[8] The most tightly bound peptide carries two ferrocenoyl (Fc) moieties[9] at the periphery of a hydrophobic binding cavity complementary in size to [60]fullerene. Since fullerene is known to exhibit a wide range of unique electrochemical and photophysical properties,[10] it is not surprising that fullerene supramolecular chemistry is receiving a great deal of attention.[11]

In this paper we describe details of the synthesis and characterization of two of the terminally-blocked, Aib-rich, rigid nonapeptide templates mentioned above, one characterized by two ferrocenoyloxybenzyl side chains (peptide **1**) and the other by two methoxybenzyl side chains (peptide **2**).

Their preferred conformations were assessed in solution by FT-IR absorption and NMR techniques and—for the latter nonapeptide in the crystal state—by X-ray diffraction. By use of steady-state, time-resolved photolytic and EPR techniques and by a mass spectrometric investigation we also definitely confirmed that the peptide template with two ferrocenoyloxybenzyl side arms is a good receptor for [60]fullerene.

[a] Prof. C. Toniolo, Dr. A. Bianco,[+] Dr. M. Crisma, Prof. M. Maggini
CSB-CNR and CMRO-CNR
Dipartimento di Chimica Organica
Università di Padova, 35131 Padova (Italy)
Fax: (+39) 049-8275239
E-mail: claudio.toniolo@unipd.it

[b] Prof. C. Corvaja, Dr. E. Sartori
Dipartimento di Chimica Fisica
Università di Padova, 35131 Padova (Italy)

[c] Dr. habil. D. M. Guldi
Radiation Laboratory
University of Notre Dame
Notre Dame, IN 46656 (USA)

[+] Current address: Institut de Biologie Moleculaire et Cellulaire
Immunologie et Chimie Thérapeutiques, UPR 9021 CNRS
67084 Strasbourg (France)

Supporting information for this article is available on the WWW under http://www.wiley-vch.de/home/chemistry/ or from the author.

  0947-6539/02/0807-1544 $ 20.00+.50/0

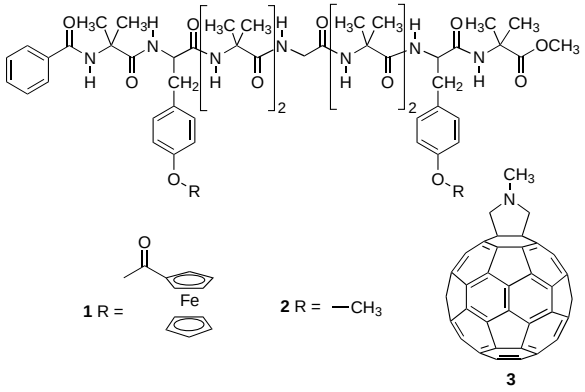

Results and Discussion

Design: Our purpose was to synthesize a peptide-based mini-receptor for [60]fullerene. To this end, we decided to prepare peptide **1**, with the following characteristics:

1) A peptide N-acylated at the N-terminus to provide an extra hydrogen-bond acceptor (the carbonyl of the blocking group), which allowed us to reduce the number of residues in the backbone by one.
2) A peptide consisting of nine residues with six (66%) C^{α}-tetrasubstituted α-amino acids to maximize the 3_{10}-helical stability without biasing the conformation toward the α-helix.[3b]
3) A peptide with two side chain-substituted L-Tyr residues separated by five intervening Aib residues, one on top of the other after two turns of the ternary helix. The two Tyr side chains were substituted with two Fc moieties, known to possess a high tendency to associate with [60]fullerene.[9] As the pitch of the 3_{10}-helix is 6.3 Å,[2a] the cleft arising from two turns of this helix should be able to host a molecule of [60]fullerene, the van der Waals diameter of which is known to be about 10 Å.[11a] Each of the two Tyr units is located one residue away from the N-/C-terminus (positions 2 and 8) to avoid involvement in peptide chain terminal fraying.[2b] 4) A peptide containing an amino acid with the smallest side chain (Gly) in position 5, one turn after and one turn before the two Tyr residues, to reduce to a minimum the steric hindrance which may disfavour fullerene encapsulation.

To demonstrate the role of the Fc moieties in fullerene encapsulation, we also synthesized a nonapeptide analogue with two side chain O-methylated L-Tyr residues (peptide **2**).

Abstract in Italian: *Sono stati sintetizzati con i classici metodi in soluzione e caratterizzati completamente due nonapeptidi bloccati alle estremità N- e C-terminali, ciascuno costituito da sei residui di Aib, uno di Gly e due di* L*-Tyr, sostituiti in catena laterale da gruppi ferrocenoilici o metilici, nelle posizioni 2 e 8. Un'analisi mediante assorbimento FT-IR e spettroscopia 2D-NMR indica che questi peptidi rigidi adottano una conformazione elicoidale di tipo 3_{10} in solventi strutturanti. Un'indagine con la diffrazione dei raggi X mostra che allo stato cristallino il nonapeptide con due residui di* L*-Tyr(Me) si avvolge in una struttura 3_{10}-elicoidale regolare destrogira. Poiché i due residui di* L*-Tyr sono separati da cinque ammino acidi, le loro due catene laterali si affacciano in soluzione dopo due giri completi dell'elica ternaria. Per mezzo di un dettagliato studio fotofisico si è dimostrato che la cavità ricca di elettroni, idrofobica e ampia, generata dalle due pareti ferrocenoilossibenziliche del templato nonapeptidico, è in grado di incapsulare una molecola di fullerene. Un'ulteriore evidenza della formazione del complesso peptide/fullerene è stata ottenuta in fase gassosa per mezzo della spettrometria di massa.*

Synthesis and characterization: The synthesis of peptides **1** and **2** started from the C-terminal H-Aib-OMe residue.[12a] Step-by-step elongation was achieved in solution by the mixed anhydride method with isobutyl chloroformate for the introduction of Boc-L-Tyr(Bzl)-OH (Boc, *tert*-butyloxycarbonyl; Bzl, benzyl) and Boc-Gly-OH and by the symmetrical anhydride method for the incorporation of the internal Aib residues.[12b] The N-terminal, N^{α}-blocked *p*BrBz-Aib (*p*BrBz, *para*-bromobenzoyl) residue was inserted via its 5(4*H*)-oxazolone derivative.[12c] The heavy atom (Br) of the *p*BrBz group was potentially useful to help in solving the phase problem in X-ray diffraction analysis should a suitable single crystal of the compound be grown. The Boc N^{α}-protecting and the Bzl side chain-protecting groups were removed by treatment with a 4N HCl/dioxane solution and by catalytic hydrogenation, respectively. Unfortunately, the bromine atom of the N^{α}-blocking group did not survive the hydrogenolysis conditions.[12d] To generate peptide **1**, the two Fc groups were attached to the deprotected Tyr side chains by use of ferrocenecarboxylic acid in a tetrahydrofuran/acetonitrile (1:1) solvent mixture in the presence of 1-[3-(dimethylamino)propyl]-3-ethyl carbodiimide and 4-(dimethylamino)pyridine.[12e] For the preparation of peptide **2**, the two methyl groups were attached to the deprotected Tyr side chains by treatment with methyl iodide in an acetone solution in the presence of potassium carbonate.

The chemical purity of peptides **1** and **2** was demonstrated by HPLC, with a Vydac reverse-phase C_{18} column. Peptides **1** and **2** and their synthetic intermediates were characterized by melting point determination, optical rotatory power, thin-layer chromatography in three different solvents and solid-state IR absorption (Table 1), amino acid analysis (Experimental Section), and ^{1}H NMR (Supporting Information).

Solution conformational analysis: The preferred conformation of the terminally blocked nonapeptides **1** and **2** was determined by combining the results of FT-IR absorption spectroscopy and one- and two dimensional NMR spectroscopy.

In the conformationally informative N–H stretching (3500–3250 cm^{-1}) and amide C=O stretching (1700–1600 cm^{-1}) regions, the FT-IR absorption spectra in $CDCl_3$ solution (not shown) exhibit a weak band at about 3425–3430 cm^{-1} (free, solvated N–H groups) accompanied by a much more intense band at 3310–3315 cm^{-1} (strongly H-bonded NH groups), and a strong band at 1662–1660 cm^{-1} (H-bonded carbonyl groups).[13] The effect of peptide concentration on the N–H stretching region is modest between 10 and 1 mM, while it is completely absent below 1 mM. This finding indicates that the 3310–3315 cm^{-1} band is

Table 1. Physical properties and analytical data for peptides **1** and **2** and their synthetic intermediates.

Peptide	M.p. [°C][a]	Recryst. solvent[b]	$[\alpha]_D^{20}$[c]	TLC[d] R_f (I)	R_f (II)	R_f (III)	IR: $\tilde{\nu}$ [cm^{-1}][e]
Boc-L-Tyr(Bzl)-Aib-OMe	76–78	EtOAc/PE	3.7	0.95	0.95	0.50	3314, 1742, 1657, 1532, 1511
Boc-Aib-L-Tyr(Bzl)-Aib-OMe	112–113	DE/PE	−25.2	0.75	0.95	0.40	3416, 3328, 1742, 1690, 1651, 1512
Boc-$(Aib)_2$-L-Tyr(Bzl)-Aib-OMe	83–85	EtOAc/PE	−10.2	0.70	0.90	0.35	3318, 1739, 1662, 1512
Boc-Gly-$(Aib)_2$-L-Tyr(Bzl)-Aib-OMe	110–112	EtOAc/PE	17.0	0.70	0.90	0.30	3321, 1730, 1660, 1511
Boc-Aib-Gly-$(Aib)_2$-L-Tyr(Bzl)-Aib-OMe	119–121	DE/PE	20.9	0.75	0.95	0.30	3314, 1739, 1660, 1532, 1511
Boc-$(Aib)_2$-Gly-$(Aib)_2$-L-Tyr(Bzl)-Aib-OMe	117–119	DE/PE	19.3	0.65	0.90	0.25	3313, 1737, 1661, 1533, 1512
Boc-L-Tyr(Bzl)-$(Aib)_2$-Gly-$(Aib)_2$-L-Tyr(Bzl)-Aib-OMe	146–148	EtOAc/PE	12.1	0.75	0.95	0.30	3313, 1737, 1660, 1530, 1511
*p*BrBz-Aib-L-Tyr(Bzl)-$(Aib)_2$-Gly-$(Aib)_2$-L-Tyr(Bzl)-Aib-OMe	148–150	EtOAc/PE	9.5	0.60	0.95	0.30	3311, 1737, 1659, 1537, 1511
Bz-Aib-L-Tyr-$(Aib)_2$-Gly-$(Aib)_2$-L-Tyr-Aib-OMe	221–223	EtOH/DE	10.4	0.30	0.90	0.05	3310, 1730, 1657, 1537, 1515
Bz-Aib-L-Tyr(Fc)-$(Aib)_2$-Gly-$(Aib)_2$-L-Tyr(Fc)-Aib-OMe (peptide **1**)	193–195	EtOAc/PE	6.1	0.60	0.95	0.25	3325, 1731, 1658, 1532
Bz-Aib-L-Tyr(Me)-$(Aib)_2$-Gly-$(Aib)_2$-L-Tyr(Me)-Aib-OMe (peptide **2**)	216–217	EtOAc/PE	7.3	0.70	0.95	0.25	3305, 1730, 1655, 1535

[a] Determined on a Leitz model Laborlux 12 apparatus. [b] EtOAc, ethyl acetate; PE, petroleum ether; DE, diethyl ether; EtOH, ethanol. [c] Determined on a Perkin–Elmer model 241 polarimeter equipped with a Haake model L thermostat: $c = 0.5$ (MeOH). [d] Silica gel glass plates (60 F-254, Merck); solvent systems: I) chloroform/ethanol 9:1; II) butan-1-ol/acetic acid/water 6:2:2; III) toluene/ethanol 7:1. The plates were developed with a UV lamp or by means of the hypochlorite/starch/iodide reaction. A single spot was observed in each case. [e] Determined in KBr pellets on a Perkin–Elmer model 580B spectrophotometer equipped with a Perkin–Elmer model 3600 IR data station and a model 660 printer.

essentially associated with intramolecular H-bonded peptide NH groups and that self-association is a phenomenon of limited significance for these peptides.[13d] The very high values for the A_H/A_F ratio (integrated intensity of the band for H-bonded NH groups relative to that for free NH groups) point to fully developed, stable helical secondary structures.[13d] Although the position of the C=O stretching band would be closer to the canonical one for the 3_{10}-helix than to that expected for the α-helix,[13e] we feel that it is not safe to discriminate between these two closely related types of helix solely on the basis of the IR absorption technique.

More detailed information on the solution conformation of peptides **1** and **2** was obtained from NMR experiments. In $CDCl_3$ solution, unambiguous assignment of all NH proton resonances was achieved by visual inspection of peak multiplicities and ROESY/TOCSY experiments. The assignment of inaccessible (or intramolecularly H-bonded) NH groups was performed by adding increasing amounts of the H-bonding acceptor solvent DMSO[14] to the $CDCl_3$ solution and by increasing the temperature in DMSO (Figure 1).

In the solvent titration study (Figure 1A), two classes of NH protons were observed: i) Aib[1] and L-Tyr(Fc)[2] NH proton resonances, both remarkably sensitive to the addition of DMSO, and ii) all other NH proton resonances, only marginally sensitive to variation of solvent composition. The presence of two DMSO-accessible NH protons at the N-terminus and seven inaccessible NH protons is strongly indicative of the onset of a 3_{10}-helical conformation for peptide **1** in $CDCl_3$ solution. Determination of the temperature coefficients of the NH proton resonances in DMSO solution[14c] confirmed the tendency of this peptide to fold in a 3_{10}-helix, although it seems that the overall helical structure would be less stable in this polar solvent at higher temperatures (Figure 1B). Again, the two amide protons at

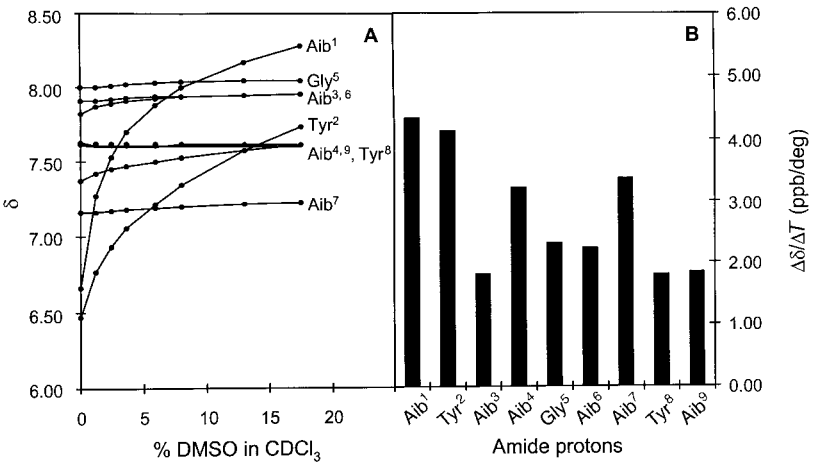

Figure 1. A) Plot of NH proton chemical shifts in the ^{1}H NMR spectrum of peptide **1** as a function of increasing percentages of DMSO (v/v) added to the $CDCl_3$ solution. B) Histogram of the chemical shift changes for the NH protons of peptide **1** as a function of heating in DMSO. Peptide concentration 1 mM.

0947-6539/02/0807-1546 $ 20.00+.50/0 *Chem. Eur. J.* **2002**, *8*, No. 7

the *N*-terminus are strongly perturbed by heating the solution. In this case, however, upon increasing the temperature, the Aib[4] and Aib[7] NH protons are also sensitive, although to a lesser extent. All these results are matched by the control peptide **2**.

To confirm the helical backbone arrangement of nonapeptide **1**, two-dimensional NMR (NOESY and ROESY) experiments were performed in $CDCl_3$ and DMSO. This analysis, besides providing unambiguous assignments for all proton resonances (except those associated with the β-CH_3 methyls of the Aib residues),[15a] showed a series of sequential ($i \rightarrow i+1$) and medium-range ($i \rightarrow i+n$, $n>1$) NOE interactions characteristic of both 3_{10}- and α-helices (Table 2).

Table 2. Interresidue NOEs found for peptide **1** in different solvents.

$CDCl_3$ and $[D_6]$DMSO				$CDCl_3/[D_2]$HFIP (1:1)			
d_{NN}	$i\rightarrow$	$i+1$		d_{NN}	$i\rightarrow$	$i+1$	
Aib[1]	HN	Tyr[2]	HN		–		
Tyr[2]	HN	Aib[3]	NH	Tyr[2]	HN	Aib[3]	NH
Aib[3]	HN	Aib[4]	HN	Aib[3]	HN	Aib[4]	HN
Aib[4]	HN	Gly[5]	HN	Aib[4]	HN	Gly[5]	HN
Gly[5]	HN	Aib[6]	HN		–		
Aib[6]	HN	Aib[7]	HN		–		
Aib[7]	HN	Tyr[8]	HN		–		
Tyr[8]	HN	Aib[9]	HN		–		
d_{NN}	$i\rightarrow$	$i+2$		d_{NN}	$i\rightarrow$	$i+2$	
Aib[1]	HN	Aib[3]	HN		–		
Tyr[2]	HN	Aib[4]	HN		–		
Gly[5]	HN	Aib[7]	HN		–		
Aib[6]	HN	Tyr[8]	HN		–		
Aib[7]	HN	Aib[9]	HN		–		
$d_{\alpha N}$	$i\rightarrow$	$i+1$		$d_{\alpha N}$	$i\rightarrow$	$i+1$	
Tyr[2]	Hα	Aib[3]	HN	Tyr[2]	HN	Aib[3]	HN
Gly[5]	Hα	Aib[6]	HN		–		
Tyr[8]	Hα	Aib[9]	HN	Tyr[8]	Hα	Aib[9]	HN
$d_{\alpha N}$	$i\rightarrow$	$i+2$		$d_{\alpha N}$	$i\rightarrow$	$i+2$	
Tyr[2]	Hα	Aib[4]	HN	Tyr[2]	Hα	Aib[4]	HN
Gly[5]	Hα	Aib[7]	HN	Gly[5]	Hα	Aib[7]	HN
$d_{\alpha N}$	$i\rightarrow$	$i+3$		$d_{\alpha N}$	$i\rightarrow$	$i+3$	
Tyr[2]	Hα	Gly[5]	HN		–		
Gly[5]	Hα	Tyr[8]	HN		–		

There is essentially only one NOE constraint [$d_{\alpha N}$ (i, $i+2$)] that is helpful for distinguishing between α- and 3_{10}-helical structures.[15b] Although only three protein amino acids are incorporated in the backbone in peptide **1**, the expected NOE cross-peaks, relating to the spatial closeness between the Tyr[2] α-CH and Aib[4] NH protons and between the Gly[5] α-CH_2 and Aib[7] NH protons, could be observed in the two-dimensional NMR spectra when using either a solvent of low polarity ($CDCl_3$) or a polar, aprotic solvent (DMSO).

An additional two-dimensional NMR experiment (ROESY) was performed in a $[D_2]$HFIP/$CDCl_3$ (1:1) mixture (HFIP = 1,1,1,3,3,3-hexafluoropropan-2-ol). Despite the acidity of HFIP, the H $\rightleftharpoons$ D amide proton exchange of N(1)H and N(2)H groups exposed to the solvent in a helical arrangement is remarkably slow, probably due to the bulkiness of the two HFIP trifluoromethyl groups. In this solvent mixture, the assignment of a few amide proton resonances turns out to be difficult because of the overlapping signals and the lack of sequential ($i \rightarrow i+1$) connectivities. Only a few $NH_i \rightarrow NH_{i+1}$ NOEs, which are characteristic of a helical structure, are observed. However, a series of cross-peaks [d_{NN} ($i \rightarrow i+1$) and $d_{\alpha N}$ ($i \rightarrow i+n$, with $n=1,2$)] from Tyr(Fc)[2] to Gly[5] does suggest that the N-terminal part of peptide **1** is still folded in a helical conformation, while all sequential NOE interactions [d_{NN} ($i \rightarrow i+1$)] are missing from Gly[5] to Aib[9]. Taken together, all these NMR results strongly support the view that the 3_{10}-helix is preferred over the α-helix in $CDCl_3$ and DMSO solutions (the latter at room temperature), while HFIP initiates a certain degree of disorder in the folded structure near the C-terminal part of peptide **1**.

Crystal-state conformational analysis: We determined the molecular and crystal structure of the acetone solvate of Bz-Aib-L-Tyr(Me)-$(Aib)_2$-Gly-$(Aib)_2$-L-Tyr(Me)-Aib-OMe (**2**, Bz = benzoyl) by X-ray diffraction. Two orthogonal views of the molecular structure are shown in Figure 2.

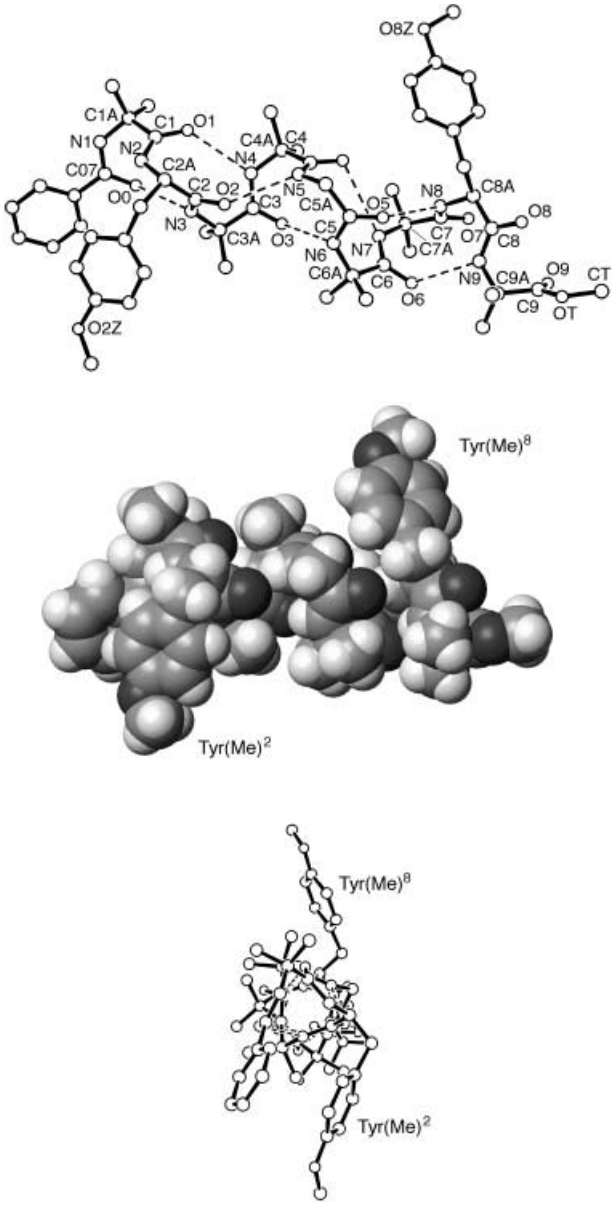

Figure 2. X-Ray diffraction structure of peptide **2**: Top) View orthogonal to the helix axis. Nitrogen and oxygen atoms are labelled. Middle) Space-filling model. Bottom) View along the helix axis. The triangular shape of the 3_{10}-helical structure is clearly visible. The intramolecular C=O···H–N H-bonds are represented by dashed lines.

Relevant backbone torsion angles are given in Table 3; the intra- and intermolecular H-bond parameters are listed in Table 4.

In general, both bond lengths and bond angles are in good agreement with previously reported values for the geometries of the benzamide[16a] and methyl ester[16b] groups, the peptide unit[16c,d] and the Aib residue.[3a, 16e]

Table 3. Selected torsion angles [°] for peptide **2** (acetone solvate).

Torsion angle		Torsion angle	
ω_0	−179.3(6)	ϕ_6	−57.2(6)
ϕ_1	−52.4(9)	ψ_6	−35.6(9)
ψ_1	−35.1(8)	ω_6	−175.4(6)
ω_1	−177.0(6)	ϕ_7	−57.8(8)
ϕ_2	−55.0(9)	ψ_7	−29.3(9)
ψ_2	−28.8(10)	ω_7	−175.5(6)
ω_2	179.1(7)	ϕ_8	−88.2(8)
ϕ_3	−54.1(10)	ψ_8	4.0(9)
ψ_3	−29.8(10)	ω_8	178.5(6)
ω_3	179.1(7)	ϕ_9	−48.8(9)
ϕ_4	−48.8(10)	"ψ_9"	134.1(7)
ψ_4	−40.1(10)	"ω_9"	−177.3(7)
ω_4	−174.9(7)		
ϕ_5	−63.6(10)		
ψ_k	−37.8(10)		
ω_5	−178.3(7)		

Table 4. Intra- and intermolecular H-bond parameters for peptide **2** (acetone solvate).

Type of H-bond	Donor D	Acceptor A	Symmetry operation	Distance [Å] D···A	Distance [Å] H···A	Angle [°] D−H···A
Intramolecular						
	N3-H	O0	x, y, z	3.002(8)	2.20	156.1
	N4-H	O1	x, y, z	2.987(8)	2.17	157.9
	N5-H	O2	x, y, z	2.972(8)	2.17	156.0
	N6-H	O3	x, y, z	3.039(8)	2.40	131.1
	N7-H	O4	x, y, z	3.261(8)	2.59	135.6
	N8-H	O5	x, y, z	3.047(7)	2.26	152.6
	N9-H	O6	x, y, z	2.986(8)	2.14	166.7
Intermolecular						
	N1-H	O9	$1-x, y+½, -z-½$	3.108(8)	2.33	150.0
	N2-H	O7	$1-x, y+½, -z-½$	3.047(7)	2.34	139.3

The first seven residues of the peptide chain are found in the right-handed helical region of the conformational map. The average values for the ϕ and ψ torsion angles[17] are −55° and −34°, closer to those expected for a 3_{10}-helix (−57°, −30°) than for an α-helix (−63°, −42°).[2a] The helical structure is stabilized by seven C=O···H−N intramolecular H-bonds of the $1 \leftarrow 4$ (β-turn[1]) type. The intramolecular O···N separations are within the limits expected for such H-bonds, except for the O4···N7 separation, which is slightly longer.[18] The first six type-III (helical) β-turns are followed by a type-I (nonhelical) β-turn (residues 7–8), which terminates the helix. This finding is related to the observation that the L-Tyr(Me)^8 conformation is slightly distorted from the helical conformation, falling in the *bridge* region of the ϕ, ψ space.[19] The C-terminal Aib residue is *semi*-extended, an unusual observation for this C^α-tetrasubstituted α-amino acid.[3c]

No significant deviations ($|\Delta\omega| > 5.1°$) of the ω torsion angles from the ideal value for *trans* planar amide, peptide and ester units (180°) are observed. The methyl ester conformation with respect to the preceding C^α–N bond is intermediate between the *synperiplanar* and *synclinal* conformations.[20a] The angle between the normals to the planes of the phenyl rings of the Bz and L-Tyr(Me)^2 moieties is 35.7(2)°. The closest intramolecular distance between two nonbonded atoms of the Bz and L-Tyr(Me)^2 phenyl rings is 4.799(8) Å.

The Tyr(Me) side chain torsion angles are: (i) χ_2^1 69.8(8)°; $\chi_2^{2,1}$ −90.4(7)°; $\chi_2^{2,2}$ 93.6(7)° for Tyr(Me)^2; (ii) χ_8^1 −70.4(7)°; $\chi_8^{2,1}$ −61.2(7)°; $\chi_8^{2,2}$ 123.3(6)° for Tyr(Me)^8. The most common side chain conformation for an L-Tyr residue in peptides[20b] is characterized by the following torsion angles: χ^1 −60° (g^-); χ^2 ±90°. The relative instability of the g^+ rotamer (χ^1 torsion angle) can be explained in terms of steric hindrance. In this conformation, the side chain C^γ atom is in a *gauche* position with respect to both heavy atom substituents on the C^α atom (N and carbonyl carbon atoms), resulting in an overall destabilization due to repulsive interactions. For aromatic amino acids, a definite preference is observed for $\chi^2 \cong \pm 90°$. In this conformation the ring is perpendicular to the plane defined by the C^α, C^β and C^γ atoms, and it is parallel to the plane defined by the N, C^α and carbonyl carbon atoms of the residue. Thus, there are no unfavourable interactions between the ring and the backbone atoms. It may be concluded that the unusual side chain conformations observed for the two L-Tyr(Me) residues [unusual χ_2^1 torsion angle for L-Tyr(Me)^2 and χ_8^2 torsion angles for L-Tyr(Me)^8] are dictated by crystal packing forces. In this three-dimensional disposition, relevant intramolecular distances between nonbonded atoms of the two L-Tyr(Me) residues are: $C^\alpha 2 \cdots C^\alpha 8$, 11.412(10) Å; $C^\beta 2 \cdots C^\beta 8$, 11.857(11) Å; $C^\gamma 2 \cdots C^\gamma 8$, 12.679(8) Å. The angle between the normals to the average planes of the phenyl rings of the L-Tyr(Me)^2 and L-Tyr(Me)^8 residues is 57.1(2)°. It is remarkable that the observed distance between the only two carbon atoms (C^γ) that might be affected by changes of the critical χ^1 torsion angle is still acceptable for [60]fullerene complexation despite this uncommon and inappropriate relative disposition of the two L-Tyr(Me) side chain.

The nonapeptide **2** molecules pack together along the *b* direction, generating a helix columnar, markedly zigzagged motif[21] stabilized by (amide) N1–H···O9=C9 (ester) and (peptide) N2–H···O7=C7 (peptide) intermolecular H-bonds of normal strength.[18] The oxygen atom of the co-crystallized solvent (acetone) molecule does not seem to be involved in any interaction with the peptide chains.

Photophysical measurements: The donor–acceptor interactions between ferrocenoyl (Fc) groups and [60]fullerene were exploited as a means to examine the ability of peptide **1** to host a fullerene molecule in a series of steady-state and time-resolved photolytic experiments. *N*-Methylfulleropyrroli-

0947-6539/02/0807-1548 $ 20.00+.50/0 *Chem. Eur. J.* **2002**, *8*, No. 7

dine **3** (MFP), rather than [60]fullerene, emerged as a convenient probe thanks to its superior solubility and fluorescence quantum yield. We reasoned that, in a structure-supporting solvent such as $CHCl_3$, the ferrocenoyloxybenzyl walls of the peptide template **1** should be able to encapsulate a fullerene moiety. In this case, the fullerene singlet excited state would be subjected to rapid intra-complex quenching by the two facing Fc units. On the other hand, addition of HFIP to $CHCl_3$ would be expected to affect the excited state dynamics and fluorescence efficiencies of MFP by partial destructuration of the helical template.

UV/Vis absorption spectroscopy: To obtain a useful insight into electronic interactions between MFP and the Fc moieties of peptide **1** in the ground state, UV/Vis absorption spectra of MFP (0.54 mM) were recorded in $CHCl_3$ and in a $CHCl_3$/HFIP (1:1 *v*/*v*) solvent mixture and compared to those obtained after addition of peptide **1** (0.31 mM). In $CHCl_3$, besides the typical absorption features of MFP, additional bands are seen at 510 and 660 nm in the presence of peptide **1** (spectrum not shown). The 510 nm band is a sensitive marker for electronic interchange between MFP and Fc, as has been demonstrated, for example, in covalently linked fullerene–Fc dyads.[22] Thus, we draw the conclusion that appreciable interactions take place between the photo- and redox-active moieties even in their ground state configurations, which can best be explained in terms of a host–guest encapsulate.

In the $CHCl_3$/HFIP (1:1) solvent mixture, these interactions, although discernible, are weak (10% in intensity relative to those seen in $CHCl_3$). It should be noted that the Fc moieties of peptide **1** exhibit their visible absorption maximum at 435 nm.[23]

Fluorescence spectroscopy: Upon excitation ($\lambda_{exc} = 355$ nm), a solution of MFP in $CHCl_3$ (0.54 mM) gives rise to a room temperature fluorescence maximum at 739 nm, formed in moderate yields (6.0×10^{-4}). However, when this solution of MFP was titrated with peptide **1**, in the concentration range between 0.1 and 0.8 mM, the fullerene fluorescence decreased progressively. The results are summarized in Figure 3.

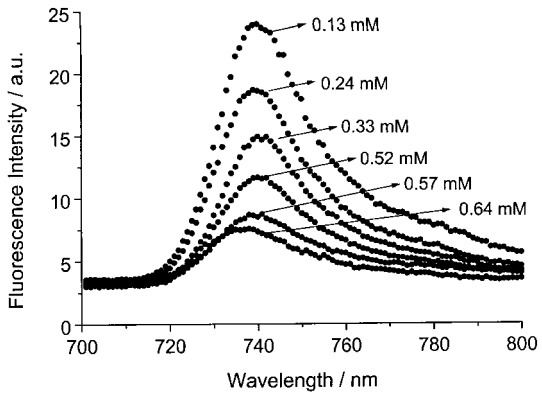

Figure 3. Emission spectra of MFP (0.54 mM) in $CHCl_3$ in the presence of variable amounts of peptide **1** (0.13–0.64 mM) with matching absorption at the 355 nm excitation wavelength.

Besides the loss of fluorescence intensity, a small red shift of the emission features (from 739 nm to 741 nm) was seen throughout the titration experiments, which implies the formation of an energetically lower-lying excited state complex between MFP and Fc.

From the plot of fluorescence intensity versus amount of peptide **1** added (Figure 4) we deduce that a peptide **1**/MFP (1:1) encapsulate is formed in $CHCl_3$. A least-squares treatment of the curve yielded a log *K* value of 4.71 ± 0.46 for the equilibrium MFP+(peptide **1**) $\rightleftharpoons$ (peptide **1**)(MFP).

The intra-complex rate constant of $2.0 \times 10^9\ s^{-1}$, which corresponds to a fluorescence lifetime of 0.50 ns, was estimated for the associated quenching process from the linear part of the graphic.

In a reference experiment, in which peptide **2**, lacking the Fc donors, was added to a $CHCl_3$ solution of MFP (0.54 mM), no significant influence on the MFP fluorescence parameters was registered, regardless of the peptide concentration, which was incrementally increased from 0.1 to 1.0 mM. This finding confirms that the Fc electron donor moieties, only present in peptide **1**, are responsible for the fluorescence quenching described above.[24]

The addition of peptide **1**, in the same concentration range (0.1–0.8 mM), to a 0.54 mM solution of MFP in a $CHCl_3$/HFIP mixture (1:1) gave rise to several differences. Firstly, and most importantly, the quenching of the MFP fluorescence is quite ineffective, despite the presence of the Fc moieties in peptide **1**. Secondly, the fluorescence decrease, as monitored over the entire concentration range, is characterized by a linear dependence (Figure 4).[25]

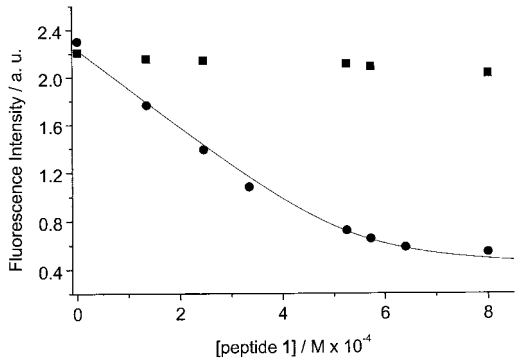

Figure 4. Plot of fluorescence intensity of MFP (0.54 mM) versus amount of peptide **1** (0.1–0.8 mM) in $CHCl_3$ (●, the full line represents the calculated curve) and in $CHCl_3$/HFIP 1:1 (■).

Time-resolved photolysis experiments, at the pico- and nanosecond timescales, were performed to shed light on the intra-complex dynamics of the quenching reactions (see above). A solution of MFP (0.54 mM) in oxygen-free $CHCl_3$ was irradiated with a laser pulse (18 ps) at $\lambda = 355$ nm. Differential absorption changes, recorded with, for instance, a 20 ps time delay, exhibited a transient maximum around 890 nm. This finding is a clear signature of the MFP singlet–singlet transition.[10d] While this event is instantaneous (<20 ps), it gives rise only rather slowly to the energetically lower-lying triplet excited state with a maximum at 700 nm. The intersystem crossing process is quantitative for MFP, with

a quantum yield of 0.98. Under the present experimental conditions, a rate of $5.75 \times 10^8\ s^{-1}$ (corresponding to a lifetime of 1.7 ns) was determined from the decay dynamics of the singlet and the grow-in of the triplet–triplet features at 890 and 700 nm, respectively.

Addition of peptide **1** (0.64 mM) to the $CHCl_3$ solution of MFP (0.54 mM) resulted in a dramatic change in the decay dynamics. A markedly shortened lifetime of the MFP singlet excited state transition (0.71 ns; Figure 5a) was estimated. This fast intra-complex deactivation agrees reasonably well with the extrapolated fluorescence lifetime. However, the spectral characteristics, recorded at the end of the picosecond timescale (6 ns), featured properties still reminiscent of the MFP triplet excited state, but in much lower yields. Indeed, an overall reduction of about 46% correlates well with the faster deactivation of the singlet excited state (59%). It is notable that the 355 nm laser pulse produces no significant amounts of Fc excited states, on account of their relative weak absorption features (<5%) at the excitation wavelength.

In a parallel experiment, in which peptide **1** was added to MFP in a $CHCl_3$/HFIP (1:1) solvent mixture, no appreciable effects were seen as far as the MFP singlet decay was concerned. The rate resembles that seen in the absence of peptide **1**: namely, $5.75 \times 10^8\ s^{-1}$. In Figure 5a the time-absorption profiles (890 nm) of a solution of MFP (0.54 mM) in the presence of peptide **1** (0.64 mM) in $CHCl_3$ and in $CHCl_3$/HFIP (1:1) are compared.

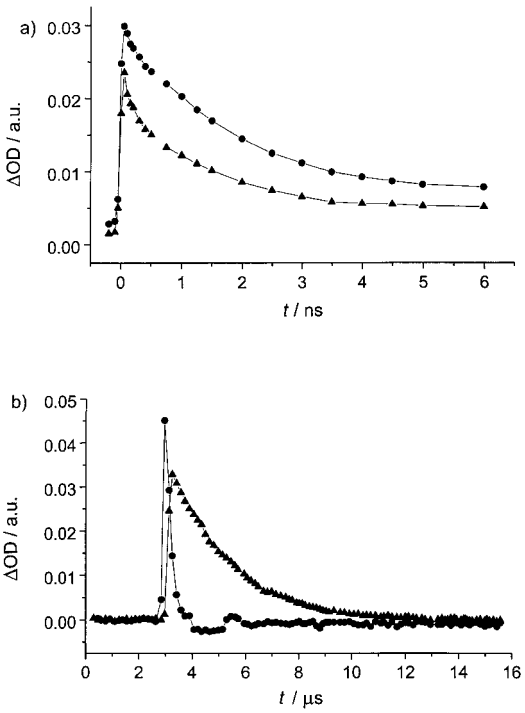

Figure 5. a) Time-absorption profiles at 890 nm for the fullerene singlet excited state decay of MFP (0.54 mM) in the presence of peptide **1** (0.64 mM) in $CHCl_3$ (▲) and $CHCl_3$/HFIP (1:1) (●). b) Time-absorption profiles at 700 nm for the fullerene triplet excited state decay of MFP (0.54 mM) in the presence of peptide **1** (0.64 mM) in $CHCl_3$ (▲) and 1:1 $CHCl_3$/HFIP (●).

In $CHCl_3$/HFIP (1:1) the MFP triplet quantum yields also failed to indicate a meaningful impact arising from the addition of peptide **1**. Essentially identical quantum yields were found in the absence or in the presence of the helical peptide receptor ($\Phi \sim 0.98$).

Similar solutions (i.e., $CHCl_3$ and $CHCl_3$/HFIP) were examined in nanosecond experiments to explore the reactivity of the MFP triplet excited state. After the conclusion of the laser pulse, the fullerene triplet with maxima at 380 and 700 nm was noted in both media, revealing a good spectral correlation with what is seen to develop over the course of the picosecond time regime. Most importantly, the triplet quantum yields corroborate the picosecond data; that is, much lower yields for the MFP and peptide **1** in $CHCl_3$ (45%) than for MFP and peptide **1** in $CHCl_3$/HFIP (1:1) (98%). Quite different triplet lifetimes were, however, derived for the two cases. Representative kinetic traces, as recorded upon excitation ($\lambda_{exc} = 355$ nm) of MFP (0.54 mM) in the presence of peptide **1** (0.64 mM) in $CHCl_3$ and $CHCl_3$/HFIP (1:1), are illustrated in Figure 5b. In $CHCl_3$ the triplet lifetime (2.6 μs) is comparable to that found in the absence of peptide **1** (~10 μs),[26] while the value in $CHCl_3$/HFIP (0.18 μs) points to a rapid triplet deactivation. Indeed, from a separate, concentration-dependent experiment we determined a diffusion-controlled, intermolecular rate constant of $2.9 \times 10^9\ M^{-1}s^{-1}$, matching that found for a reaction of MFP with a Fc reference ($2.0 \times 10^9\ M^{-1}s^{-1}$) under closely related experimental conditions. This observation supports the view that destructuration of the peptide template hampers encapsulation of MFP in the $CHCl_3$/HFIP mixture. Accordingly, any quenching is limited to a truly intermolecular process.

This result in turn evoked the working hypothesis that removal of the protic fluoroalcohol component from $CHCl_3$/HFIP should ultimately restore the peptide template and result again in MFP encapsulation. To prove this, we removed HFIP from the solvent mixture and examined the fullerene fluorescence. Indeed, a substantial decrease in emission quenching, the magnitude of which was now comparable to that described for $CHCl_3$ (see above), suggests the successful reformation of the host–guest encapsulate. Furthermore, further addition of the more volatile HFIP component once more resulted in the activation of the emission. Unequivocally, this finding confirms the reversible transformation and thus the topological control over the peptide template. Important for the performance of these fluorescent probes is the fact that no notable deviation from reversibility was found after this activation/deactivation cycle (i.e., addition and removal of HFIP) had been followed up to ten times.

EPR measurements: Time-resolved (TR) EPR experiments were performed to complement the steady-state and flash photolysis results. Irradiation ($\lambda = 532$ nm) of a $CHCl_3$ solution of MFP (0.5 mM) at room temperature produced the EPR signal of triplet excited MFP. The signal decay (not shown) is fitted by the sum of two exponential functions, characterized by the time constants $\tau_1 = 0.95$ μs and $\tau_2 = 9.5$ μs. The τ_1 term relates to the spin lattice relaxation, which brings the triplet signal, initially polarized in enhanced absorption, to thermal equilibrium. The τ_2 term is the triplet lifetime.

0947-6539/02/0807-1550 $ 20.00+.50/0 *Chem. Eur. J.* **2002**, *8*, No. 7

Addition of 0.5 mM peptide **1** to the $CHCl_3$ solution deeply affects the triplet evolution, the decay becoming much faster and monoexponential. A lifetime of 0.43 μs could be measured. An analogous monoexponential decay, with a slightly shorter time constant ($\tau = 0.24$ μs), was recorded when ferrocene (0.5 mM) was added to a $CHCl_3$ solution of MFP (0.5 mM).

In $CHCl_3$/HFIP (1:1) in the presence of 0.5 mM peptide **1**, the MFP triplet excited state decay is biexponential, the triplet quenching rate being sufficiently lower than the spin lattice relaxation ($\tau_1 = 0.49$ μs, $\tau_2 = 1.37$ μs). Indeed, the triplet excited state decay is slower than that previously measured for MFP-peptide **1** in pure $CHCl_3$.

In all cases the rising time of the TR-EPR signal matches the time resolution of the EPR instrumentation.

These results, which apparently contradict those from optical measurements, may be accounted for by the much higher excitation light intensity used in TR-EPR experiments. Thus, only triplet states arising from uncomplexed MFP are monitored, and decay of these is governed by intermolecular diffusion-controlled reactions. Since HFIP is more viscous than $CHCl_3$, a lower diffusion limit is to be expected for the $CHCl_3$/HFIP (1:1) solvent mixture.

Mass spectrometric studies: The formation of the peptide **1**·MFP (1:1) complex was confirmed in the gas phase by API-ToF (atmospheric pressure ionization-time of flight detection) mass spectrometry in the positive ion mode. The spectrum (not shown, see Supporting Information) recorded from a mixture (1:2) of peptide **1** and MFP, dissolved in a $CHCl_3$/MeOH (2:1) solvent mixture, displayed an intense peak at *m*/*z* 2232.7, which corresponds to the supramolecular ion $[\mathbf{1}\cdot MFP+H]^+$. The peaks at *m*/*z* 1476.6 and *m*/*z* 1454.6 can be assigned to $[\mathbf{1}+Na^+]^+$ and $[\mathbf{1}+H]^+$, respectively. The base peak was detected at *m*/*z* 778, which corresponds to $[MFP+H]^+$.

Conclusion

We have designed and synthesized a helical, Aib-rich nonapeptide (**1**), potentially able to encapsulate a [60]fullerene moiety. A FT-IR absorption and NMR investigation clearly demonstrated that the peptide is folded in a stable 3_{10}-helix under structure-supporting conditions. We have also synthesized a control nonapeptide (**2**) in which the two electron-rich ferrocenoyloxybenzyl side chains of (**1**) are replaced by two methoxybenzyl side chains. An X-ray diffraction analysis of this latter peptide unambiguously proved the high tendency of the −C(=O)-Aib-L-Tyr-$(Aib)_2$-Gly-$(Aib)_2$-L-Tyr-Aib− backbone to adopt a regular, 3_{10}-helical conformation.

Our photophysical investigation confirms that, in $CHCl_3$, the ferrocenoyloxybenzyl walls of the peptide template **1** do indeed host the fullerene moiety of MFP. Upon photoexcitation the singlet excited state of MFP is therefore primed for a rapid intra-complex deactivation by the ferrocenoyl groups. Conversely, in the $CHCl_3$/HFIP solvent mixture, which disfavours the formation of a host–guest complex, no evidence for intra-complex processes was obtained. Instead, MFP reacts with ferrocene in its triplet excited state, predominantly by diffusion-controlled dynamics.

Evidence for the onset of a peptide **1**·MFP superstructure was also provided by a mass spectrometric investigation in the gas phase.

Compound **1** is, to our knowledge, the first peptide-based (1:1) mini-receptor reported for [60]fullerene. In their classical paper, Friedman et al.[27] proposed that a [60]fullerene molecule could be sandwiched snugly into the hydrophobic cavity generated by the HIV protease dimer (1:2 stoichiometry).

Experimental Section

Materials: The physical properties of and the analytical data for peptides **1** and **2** and their synthetic intermediates are listed in Table 1. In addition, the following results for the amino acid analyses (C. Erba model 3A-30) were obtained. Boc-L-Tyr(Bzl)-Aib-OMe: Tyr 0.98, Aib 1.02; Boc-Aib-L-Tyr(Bzl)-Aib-OMe: Tyr 0.89, Aib 2.11; Boc-$(Aib)_2$-L-Tyr(Bzl)-Aib-OMe: Tyr 0.93, Aib 3.07; Boc-Gly-$(Aib)_2$-L-Tyr(Bzl)-Aib-OMe: Tyr 0.91, Aib 3.09, Gly 1.00; Boc-Aib-Gly-$(Aib)_2$-L-Tyr(Bzl)-Aib-OMe: Tyr 0.93, Aib 4.06, Gly 1.01; Boc-$(Aib)_2$-Gly-$(Aib)_2$-L-Tyr(Bzl)-Aib-OMe: Tyr 0.88, Aib 5.18, Gly 0.94; Boc-L-Tyr(Bzl)-$(Aib)_2$-Gly-$(Aib)_2$-L-Tyr(Bzl)-Aib-OMe: Tyr 1.87, Aib 5.13, Gly 1.00; *p*BrBz-Aib-L-Tyr(Bzl)-$(Aib)_2$-Gly-$(Aib)_2$-L-Tyr(Bzl)-Aib-OMe: Tyr 1.92, Aib 6.06, Gly 1.02; Bz-Aib-L-Tyr(Bzl)-$(Aib)_2$-Gly-$(Aib)_2$-L-Tyr(Bzl)-Aib-OMe: Tyr 1.93, Aib 6.16, Gly 0.91; Bz-Aib-L-Tyr(Fc)-$(Aib)_2$-Gly-$(Aib)_2$-L-Tyr(Fc)-Aib-OMe (peptide **1**): Tyr 1.90, Aib 6.19, Gly 0.91; Bz-Aib-L-Tyr(Me)-$(Aib)_2$-Gly-$(Aib)_2$-L-Tyr(Me)-Aib-OMe (peptide **2**): Tyr 1.91, Aib 6.09, Gly 1.00. [60]Fullerene was purchased from BuckyUSA, Houston, TX, USA (99.5 %). All other reagents were used as purchased. *N*-Methyl fulleropyrrolidine (**3**) was prepared as described.[28] All solvents for synthesis were distilled prior to use. The solvents employed for the UV/Vis absorption and photophysical measurements were commercially available, spectroscopic grade solvents which were carefully deoxygenated prior to use.

FT-IR absorption: FT-IR absorption spectra were recorded with a Perkin–Elmer model 1720X spectrophotometer, flushed with nitrogen and equipped with a sample shuttle device, at 2 cm^{-1} nominal resolution, averaging 100 scans. Solvent (baseline) spectra were recorded under the same conditions. Cells with path lengths of 0.1, 1.0 and 10 mm (with CaF_2 windows) were used. Spectrograde [D]chloroform (99.8 % D) was purchased from Merck.

^{1}H NMR spectra: ^{1}H NMR spectra were recorded with a Bruker model AM 400 spectrometer. Measurements were carried out in $CDCl_3$ (99.96 % D; Merck), [D_6]DMSO (99.96 % D; Fluka) and [D_2]HFIP (98 % D; Cambridge Isotope Laboratories) with tetramethylsilane as the internal standard.

Mass spectrometric study: API-ToF (atmospheric pressure ionization-time of flight detection) mass spectrometry was carried out with an Applied Biosystems Mariner 5220 mass spectrometer set up for positive ion detection. Peptide **1** and MFP were dissolved in a chloroform/methanol mixture (2:1) at concentrations of 1.0×10^{-5} M and 2.0×10^{-5} M, respectively. This solution was used for direct injection into the spectrometer. The nozzle temperature was adjusted at 100 °C, the nozzle potential at 60 V and the spray tip potential at 4200 V.

X-Ray diffraction: Single crystals of Bz-Aib-L-Tyr(Me)-$(Aib)_2$-Gly-$(Aib)_2$-L-Tyr(Me)-Aib-OMe (**2**) acetone solvate were grown from acetone/*n*-hexane by vapour diffusion. Cell parameters were obtained by least-squares refinement of the angular setting of 25 carefully centred reflections in the 12–24° θ range. Data collection was performed with a Philips PW 1100 four-circle diffractometer, using graphite monochromated $Cu_{K\alpha}$ radiation.

The phases of thirteen *hk0* reflections were eventually assigned by application of the SHELX 76 program[29a] to a data subset with $l = 0$, in the rectangular space group *p2gg*, which corresponds to a centrosymmetric projection of the actual three-dimensional space group $P2_12_12_1$. The

introduction of such phases as a lead for the direct methods of the SHELXS 86 program,[29b] with the full dataset, permitted the location of all non-H atoms of the peptide molecule. The atomic positions of the disordered, co-crystallized acetone molecule were recovered from a subsequent difference Fourier map.

Refinement was carried out by full-matrix-block, least-squares on F^2, using all data, by application of the SHELXL 97 program,[29c] with all non-H atoms anisotropic, and allowing the positional parameters and the anisotropic displacement parameters of the non-H atoms to refine at alternate cycles. The methoxy group of the Tyr(Me)[8] residue is disordered. Its CH_3 group was refined on two positions (C8Z′ and C8Z″), with population parameters of 0.58 and 0.42, respectively. The co-crystallized acetone molecule is also disordered (except for the carbonyl carbon atom). It was eventually modelled on two sites, rotated by about 60°, each with a population parameter of 0.50. Restraints were applied to the bond distances as well as to the anisotropic displacement parameters (the latter restraint to approach isotropic behaviour) of the disordered groups. A planarity restraint was imposed to each position of the disordered acetone molecule. All phenyl rings were constrained to the idealized geometry. The H-atoms were calculated at idealized positions and refined as riding with U_{iso} set equal to 1.2 (or 1.5 for the CH_3 groups) times the U_{eq} of the parent atom. Relevant crystallographic data and structure refinement parameters are listed in Table 5.

Table 5. Crystal data and structure refinement for peptide **2**.

empirical formula	$C_{57}H_{81}N_9O_{14}$
M_W [amu]	1116.3
T [K]	293(2)
λ [Å]	1.54178 ($Cu_{K\alpha}$)
crystal system	orthorhombic
space group	$P2_12_12_1$
a [Å]	15.208(2)
b [Å]	28.476(4)
c [Å]	14.553(2)
α [°]	90
β [°]	90
γ [°]	90
V [Å^3]	6302.4(15)
Z	4
ρ_{calcd} [g cm^{-3}]	1.176
μ [mm^{-1}]	0.70
$F(000)$	2392
crystal size [mm]	$0.50 \times 0.35 \times 0.30$
θ range [°]	3.29 to 59.98
index ranges	$0 \le h \le 17$
	$0 \le k \le 31$
	$0 \le l \le 16$
reflections collected	5187
independent reflections	5184
refinement method	full-matrix-block least-squares on F^2
data/restraints/parameters	5184/78/722
goodness of fit (on F^2)	0.95
final R indices [$I > 2\sigma(I)$]	$R_1 = 0.074$, $wR_2 = 0.186$
R indices (all data)	$R_1 = 0.141$, $wR_2 = 0.230$
largest diff. peak and hole [e Å^{-3}]	0.292; −0.329

Crystallographic data (excluding structure factors) for the structure reported in this paper have been deposited with the Cambridge Crystallographic Data Centre as supplementary publication no. CCDC-166805. Copies of the data can be obtained free of charge on application to CCDC, 12 Union Road, Cambridge CB2 1EZ, UK (fax: (+44) 1223–336–033; e-mail: deposit@ccdc.cam.ac.uk).

Photophysical measurements: Emission spectra were recorded with a SLM 8100 spectrofluorimeter. The experiments were performed at room temperature. The MFP fluorescence was recorded by using a 570 nm long-pass filter in the emission path in order to eliminate the interference from the solvent and stray light. Each spectrum was an average of at least five individual scans and the appropriate corrections were applied.

Picosecond laser flash photolysis experiments were carried out with 355 nm laser pulses from a mode-locked, Q-switched Quantel YG-501 DP Nd/YAG laser system (pulse width 18 ps, 2–3 mJ pulse^{-1}). The white continuum picosecond probe pulse was generated by passing the fundamental output through a D_2O/H_2O solution. Nanosecond laser flash photolysis experiments were performed with laser pulses from a Quanta-Ray CDR Nd/YAG system (355 nm, 6 ns pulse width) in a front face excitation geometry. A Xe lamp was triggered synchronously with the laser. A monochromator (SPEX) in combination with either a Hamamatsu R 5108 photomultiplier or a fast InGaAs diode was employed to monitor transient absorption spectra. The photomultiplier output was digitized with a Tektronix 7912 AD programmable digitizer.

EPR measurements: Time-resolved EPR spectra were recorded with a Bruker ER 200 D X-band spectrometer. The second harmonic (λ = 532 nm) of a Nd/YAG laser (Quantel) was used for the excitation. A Lecroy 9450A digital oscilloscope was used to collect and average the transient signals. Other experimental details were reported previously.[30]

Acknowledgement

We wish to thank Dr. D. Dal Zoppo (CRIBI-Padova) for API-ToF MS data and Dr. F. Mancin (Univ. Padova) for the helpful discussions. This work was in part supported by the Office of Basic Energy Sciences of the Department of Energy, USA (Contribution No. NDRL-4362), by the Italian CNR through CMRO (legge 95/95) and by the Italian MIUR (contract No. MM03198284). This is document 27810 from the Notre Dame Radiation Laboratory. M.M. and D.G. thank NATO for a travel grant (Grant No. CRG960099).

[1] a) C. M. Venkatachalam, *Biopolymers* **1968**, *6*, 1425–1436; b) C. Toniolo, *CRC Crit. Rev. Biochem.* **1980**, *9*, 1–44; c) G. D. Rose, L. M. Gierasch, J. A. Smith, *Adv. Protein Chem.* **1985**, *37*, 1–109.

[2] a) C. Toniolo, E. Benedetti, *Trends Biochem. Sci.* **1991**, *16*, 350–353; b) K. A. Bolin, G. L. Millhauser, *Acc. Chem. Res.* **1999**, *32*, 1027–1033.

[3] a) Y. Paterson, S. M. Rumsey, E. Benedetti, G. Nemethy, H. A. Scheraga, *J. Am. Chem. Soc.* **1981**, *103*, 2947–2955; b) I. Karle, P. Balaram, *Biochemistry* **1990**, *29*, 6747–6756; c) C. Toniolo, E. Benedetti, *Macromolecules* **1991**, *24*, 4004–4009.

[4] a) N. Voyer, J. Lamothe, *Tetrahedron* **1995**, *51*, 9241–9284; b) C. Toniolo, F. Formaggio, M. Crisma, G. Valle, W. H. J. Boesten, H. E. Schoemaker, J. Kamphuis, P. A. Temussi, E. L. Becker, G. Precigoux, *Tetrahedron* **1993**, *49*, 3641–3653; c) C. Toniolo, A. Bianco, F. Formaggio, M. Crisma, G. M. Bonora, E. Benedetti, V. Del Duca, M. Saviano, R. Di Blasio, C. Pedone, A. Aubry, *Bioorg. Med. Chem.* **1995**, *3*, 1211–1221.

[5] a) C. Toniolo, E. Valente, F. Formaggio, M. Crisma, G. Pilloni, C. Corvaja, A. Toffoletti, G. V. Martinez, M. P. Hanson, G. L. Millhauser, C. George, J. L. Flippen-Anderson, *J. Pept. Sci.* **1995**, *1*, 45–57; b) P. Hanson, G. Millhauser, F. Formaggio, M. Crisma, C. Toniolo, *J. Am. Chem. Soc.* **1996**, *118*, 7618–7625; c) C. Toniolo, F. Formaggio, M. Crisma, J. P. Mazaleyrat, M. Wakselman, C. George, J. R. Deschamps, J. L. Flippen-Anderson, B. Pispisa, M. Venanzi, A. Palleschi, *Chem. Eur. J.* **1999**, *5*, 2254–2264; d) C. Corvaja, E. Sartori, A. Toffoletti, F. Formaggio, M. Crisma, C. Toniolo, J. P. Mazaleyrat, M. Wakselman, *Chem. Eur. J.* **2000**, *6*, 2775–2782.

[6] a) G. Basu, M. Kubasik, D. Anglos, B. Secor, A. Kuki, *J. Am. Chem. Soc.* **1990**, *112*, 9410–9411; b) G. Basu, D. Anglos, A. Kuki, *Biochemistry* **1993**, *32*, 3067–3076; c) D. Anglos, V. Bindra, A. Kuki, *J. Chem. Soc. Chem. Commun.* **1994**, 213–215; d) E. Galoppini, A. M. Fox, *J. Am. Chem. Soc.* **1996**, *118*, 2289–2300; e) A. M. Fox, E. Galoppini, *J. Am. Chem. Soc.* **1997**, *119*, 5277–5285; f) F. Donald, G. Hungerford, D. J. S. Birch, B. D. Moore, *J. Chem. Soc. Chem. Commun.* **1995**, 313–314; g) G. Hungerford, M. Martinez-Insua, D. J. S. Birch, B. D. Moore, *Angew. Chem.* **1996**, *108*, 356–359; *Angew. Chem. Int. Ed. Engl.* **1996**, *35*, 326–329; h) M. Sisido, Y. Ishikawa, M. Harada, S. Tazuke, *Macromolecules* **1991**, *24*, 3993–3998; i) M. Sisido, Y. Ishikawa, M. Harada, K. Itoh, *Macromolecules* **1991**, *24*, 3999–4003.

  0947-6539/02/0807-1552 $ 20.00+.50/0

[7] a) P. Rossi, F. Felluga, P. Tecilla, F. Formaggio, M. Crisma, C. Toniolo, P. Scrimin, *Biopolymers* (*Pept. Sci.*) **2000**, *55*, 496–501; b) C. Sissi, P. Rossi, F. Felluga, F. Formaggio, M. Palumbo, P. Tecilla, C. Toniolo, P. Scrimin, *J. Am. Chem. Soc.* **2001**, *123*, 3169–3170; c) P. Rossi, F. Felluga, P. Tecilla, F. Formaggio, M. Crisma, C. Toniolo, P. Scrimin, *J. Am. Chem. Soc.* **1999**, *121*, 6948–6949.

[8] A. Bianco, F. Gasparrini, M. Maggini, D. Misiti, A. Polese, M. Prato, G. Scorrano, C. Toniolo, C. Villani, *J. Am. Chem. Soc.* **1997**, *119*, 7550–7554.

[9] a) J. D. Crane, P. B. Hitcock, H. W. Kroto, R. Taylor, D. R. M. Walton, *J. Chem. Soc. Chem. Commun.* **1992**, 1764–1765; b) P. R. Birkett, J. D. Crane, P. B. Hitcock, H. W. Kroto, M. F. Meidine, R. Taylor, D. R. M. Walton, *J. Mol. Struct.* **1993**, *292*, 1–8.

[10] a) *Fullerenes and Related Structures* in Topics in Current Chemistry, *Vol. 199* (Ed.: A. Hirsch), Springer, Berlin, **1999**; b) *Fullerenes*: *Chemistry*, *Physics*, *and Technology* (Ed.: K. Kadish), Wiley, New York, **2000**; c) L. Echegoyen, L. E. Echegoyen, *Acc. Chem. Res.* **1998**, *31*, 593–601; d) D. M. Guldi, M. Prato, *Acc. Chem. Res.* **2000**, *33*, 695–703.

[11] a) F. Diederich, M. Gomez-Lopez, *Chem. Soc. Rev.* **1998**, *28*, 263–277; b) M. J. Hardie, C. L. Raston, *J. Chem. Soc. Chem. Commun.* **1999**, 1153–1163; c) M. Yanase, T. Haino, Y. Fukazawa, *Tetrahedron Lett.* **1999**, *40*, 2781–2784; c) K. Tashiro, T. Aida, J.-Y. Zheng, K. Kinbara, K. Saigo, S. Sakamoto, K. Yamaguchi, *J. Am. Chem. Soc.* **1999**, *121*, 9477–9478; d) P. D. W. Boyd, M. C. Hodgson, C. E. F. Rickard, A. G. Oliver, L. Chaker, P. J. Brothers, R. D. Bolskar, F. S. Tham, C. A. Reed, *J. Am. Chem. Soc.* **1999**, *121*, 10487–10495; e) J.-F. Nierengarten, L. Oswald, J.-F. Eckert, J.-F. Nicoud, N. Armaroli, *Tetrahedron Lett.* **1999**, *40*, 5681–5684; f) C. Zonta, S. Cossu, O. De Lucchi, *Eur. J. Org. Chem.* **2000**, 1965–1971; g) A. Ikeda, T. Hatano, S. Shinkai, T. Akiyama, S. Yamada, *J. Am. Chem. Soc.* **2001**, *123*, 4855–4856.

[12] a) M. T. Leplawy, D. S. Jones, G. W. Kenner, R. C. Sheppard, *Tetrahedron* **1960**, *11*, 39–51; b) A. Bianco, Ph.D. thesis, University of Padova (Italy), **1995**; c) G. Valle, M. Crisma, C. Toniolo, *Z. Kristallogr.* **1986**, *175*, 73–83; d) M. K. Anwer, R. A. Porter, A. F. Spatola, *Int. J. Pept. Protein Res.* **1987**, *30*, 489; e) E. F. V. Scriven, *Chem. Soc. Rev.* **1983**, *12*, 129–161.

[13] a) M. T. Cung, M. Marraud, J. Neel, *Ann. Chim.* (*France*) **1972**, *7*, 183–209; b) C. P. Rao, R. Nagaraj, C. N. R. Rao, P. Balaram, *Biochemistry* **1980**, *19*, 425–431; c) G. M. Bonora, C. Mapelli, C. Toniolo, R. R. Wilkening, E. S. Stevens, *Int. J. Biol. Macromol.* **1984**, *6*, 179–188; d) C. Toniolo, G. M. Bonora, V. Barone, A. Bavoso, E. Benedetti, B. Di Blasio, P. Grimaldi, F. Lelj, V. Pavone, C. Pedone, *Macromolecules* **1985**, *18*, 895–902; e) D. F. Kennedy, M. Crisma, C. Toniolo, D. Chapman, *Biochemistry* **1991**, *30*, 6541–6548.

[14] a) D. Martin, H. G. Hauthal, *Dimethyl Sulphoxide*, van Nostrand–Reinhold, Wokingham, UK, **1975**; b) K. D. Kopple, M. Ohnishi, A. Go, *Biochemistry* **1969**, *8*, 4087–4095; c) J. D. Augspurger, V. A. Bindra, H. A. Scheraga, A. Kuki, *Biochemistry* **1995**, *34*, 2566–2576.

[15] a) R. Gratias, R. Konat, H. Kessler, M. Crisma, G. Valle, A. Polese, F. Formaggio, C. Toniolo, Q. B. Broxterman, J. Kamphuis, *J. Am. Chem. Soc.* **1998**, *120*, 4763–4770; b) K. Wutrich, *NMR of Proteins and Nucleic Acids*, Wiley, New York, **1986**, pp. 192–196.

[16] a) P. Chakrabarti, J. D. Dunitz, *Helv. Chim. Acta* **1982**, *65*, 1555–1562; b) W. B. Schweizer, J. D. Dunitz, *Helv. Chim. Acta* **1982**, *65*, 1547–1554; c) E. Benedetti, in *Chemistry and Biochemistry of Amino Acids*, *Peptides*, *and Proteins*, *Vol. 6* (Ed.: B. Weinstein), Dekker, New York, **1982**, pp. 105–184; d) T. Ashida, Y. Tsunogae, I. Tanaka, T. Yamane, *Acta Crystallogr. Sect. B* **1987**, *43*, 212–218; e) G. Valle, M. Crisma, F. Formaggio, C. Toniolo, G. Jung, *Liebigs Ann.* **1985**, 1055–1060.

[17] IUPAC-IUB Commission on Biochemical Nomenclature, *J. Mol. Biol.* **1970**, *52*, 1–17.

[18] a) C. Ramakrishnan, N. Prasad, *Int. J. Protein Res.* **1971**, *3*, 209–231; b) R. Taylor, O. Kennard, W. Versichel, *Acta Crystallogr. Sect. B* **1984**, *40*, 280–288; c) C. H. Gorbitz, *Acta Crystallogr. Sect. B* **1989**, *45*, 390–395.

[19] S. S. Zimmerman, M. S. Pottle, G. Nemethy, H. A. Scheraga, *Macromolecules* **1977**, *10*, 1–9.

[20] a) J. D. Dunitz, P. Strickler in *Structural Chemistry and Molecular Biology* (Eds.: A. Rich, N. Davidson), Freeman, San Francisco, **1968**, pp. 595–602; b) E. Benedetti, G. Morelli, G. Nemethy, H. A. Scheraga, *Int. J. Pept. Protein Res.* **1983**, *22*, 1–15.

[21] I. L. Karle, *Acta Crystallogr. Sect. B* **1992**, *48*, 341–356.

[22] D. M. Guldi, M. Maggini, G. Scorrano, M. Prato, *J. Am. Chem. Soc.* **1997**, *119*, 974–980.

[23] The presence of just HFIP causes a small blue shift of the MFP transition in the visible region (i.e., from 430 nm to 428 nm).

[24] The room temperature studies were complemented by measurements in a frozen matrix at 77 K. Interestingly, similar characteristics were detected; that is, fluorescence quenching plus red shift. More importantly, the relationship between fluorescence intensity and peptide concentration reveals the same nonlinear dependence as seen in the room temperature titrations. The immiscibility of $CHCl_3$ and HFIP at 77 K, however, restricts the corresponding $CHCl_3$/HFIP studies to room temperature measurements.

[25] Although the quenching efficiency in $CHCl_3$/HFIP is reduced by one order of magnitude, it is in line with our earlier conclusion on the existence of ground-state interactions between MFP and peptide **1**. The weaker interactions in $CHCl_3$/HFIP are further substantiated by the position of the fluorescence maximum, which, unlike the findings in neat $CHCl_3$, shows no red shift even upon addition of 6.4 mM peptide **1**.

[26] The triplet quenching is due to uncomplexed MFP.

[27] S. H. Friedman, D. L. De Camp, R. P. Sijbesma, G. Srdanov, F. Wudl, G. L. Kenyon, *J. Am. Chem. Soc.* **1993**, *115*, 6506–6509.

[28] M. Maggini, G. Scorrano, M. Prato, *J. Am. Chem. Soc.* **1993**, *115*, 9798–9799.

[29] a) G. M. Sheldrick, SHELX 76, Program for the refinement of crystal structures, University of Göttingen, Göttingen (Germany), **1976**; b) G. M. Sheldrick, SHELX 86, Program for the solution of crystal structures, University of Göttingen, Göttingen (Germany), **1986**; c) G. M. Sheldrick, SHELX 97, Program for the solution of crystal structures, University of Göttingen, Göttingen (Germany), **1997**.

[30] C. Corvaja, L. Franco, M. Mazzoni, *Appl. Magn. Reson.* **2001**, *20*, 71–83.

Received: August 8, 2001 [F3481]